AGU PUBLICATIONS

Geophysical Research Letters

RESEARCH LETTER
10.1002/2017GL075772

Key Points:
- The subtropical surface salinity maximum water in the North Atlantic has expanded toward North since 1979
- The expansion shifted and expanded the ventilation zone, leading to an increased production of the subtropical underwater
- The underwater has become broader, deeper, and saltier, and the changes are particularly noted on the northern/western edges of the core

Supporting Information:
- Supporting Information S1

Correspondence to:
L. Yu,
lyu@whoi.edu

Citation:
Yu, L., Jin, X., & Liu, H. (2018). Poleward shift in ventilation of the North Atlantic subtropical underwater. *Geophysical Research Letters*, *45*, 258–266. https://doi.org/10.1002/2017GL075772

Received 21 SEP 2017
Accepted 20 DEC 2017
Accepted article online 27 DEC 2017
Published online 15 JAN 2018

Poleward Shift in Ventilation of the North Atlantic Subtropical Underwater

Lisan Yu[1], Xiangze Jin[1], and Hao Liu[1,2]

[1]Department of Physical Oceanography, Woods Hole Oceanographic Institution, Woods Hole, MA, USA, [2]College of Physical and Environmental Oceanography, Ocean University of China, Qingdao, China

Abstract We report the findings that the sea surface salinity maximum (SSS-max) in the North Atlantic has poleward expanded in recent decades and that the expansion is a main driver of the decadal changes in subtropical underwater (STUW). We present observational evidence that the STUW ventilation zone (marked by the location of the 36.7 isohaline) has been displaced northward by1.2 ± 0.36° latitude for the 34 year (1979–2012) period. As a result of the redistribution of the SSS-max water, the ventilation zone has shifted northward and expanded westward into the Sargasso Sea. The ventilation rate of STUW has increased, which is attributed to the increased lateral induction of the sloping mixed layer. STUW has become broader, deeper, and saltier, and the changes are most pronounced on the northern and western edges of the high-saline core.

Plain Language Summary The subtropical high pressure of the descending branch of the Hadley circulation is located between 20° and 40° of both north and south latitudes. Within the zone, a pool of sea surface salinity maximum (SSS-max) exists in responding to the excess of evaporation over precipitation. Among all SSS-max centers, the North Atlantic SSS-max is highest, in excess of 37. In the past 50 years, the salinities in the subtropical North Atlantic have increased, and the trend is seen as an ocean supporting evidence of the "dry-gets-drier and wet-gets-wetter" paradigm , indicating that the global water cycle amplifies as a consequence of the increase in water vapor transport. However, we hypothesize in this study that the salinity increase is due to the poleward expansion of the SSS-max center in association with the widening of the tropics in the recent decades and that the expansion has shifted the ventilation zone of subtropical underwater—a high-saline water mass in the upper 50–300 m. The subtropical underwater has become broader, deeper, and saltier. Because of its connection to the tropical and subpolar regions via interior pathways, the change of subtropical underwater could have profound impacts on both the equatorial thermocline and the North Atlantic Deep Water.

1. Introduction

The subtropical high pressure of the descending branch of the Hadley circulation is located between 20° and 40° of both north and south latitudes. Within this zone, the excess of evaporation over precipitation ($E > P$), together with surface convergence of the wind-driven Ekman flow, leads to a pool of sea surface salinity maximum (SSS-max) in the subtropical gyres of the world's ocean. Of all SSS-max centers, the North Atlantic SSS-max is the highest, in excess of 37 and also the most studied (Bingham et al., 2014; Bryan & Bachman, 2014; Gordon et al., 2015; Reverdin et al., 2007). During the early spring when the mixed layer warms up and shoals, the subduction of the surface high-salinity water leads to the formation of a distinct salinity maximum at the depths of 50–300 m. This intermediate water mass is referred to as subtropical underwater (STUW) (e.g., O'Connor et al., 2005) or salinity maximum water (e.g., Blanke et al., 2002; Worthington, 1976).

Subduction is the mass flux from the base of the mixed layer to the permanent pycnocline, and the process is part of the ventilation of the interior ocean (Luyten et al., 1983). Ventilation of the STUW in the North Atlantic typically occurs in latitudes between 20° and 30°N (Worthington, 1976). The outcrop salinity ranges from 36.7 to 37.2 and potential temperature from 20.4 to 22.2°C (O'Connor et al., 2005), equivalent to 25.6–26.3 kg m^{-3} density outcrop lines. After descending into the ocean interior, STUW is advected southward and southwestward by the Sverdrup circulation. Hydrographic surveys have shown STUW entering the Caribbean Sea (Hernández-Guerra & Joyce, 2000) and appearing in the Straits of Florida (Schmitz & Richardson, 1991) at depths of ~150–300 m. Over the past decades, a few sustained biogeochemical and ecological time series stations have been established in the western subtropical basin, including the Bermuda Atlantic Time-series Study (BATS,

31.7°N, 64.2°W) and Hydrostation "S" (32.1°N, 64.4°W). Montes et al. (2016) reported decadal-scale variability of STUW at these stations, featuring a reduction in the dissolved oxygen concentrations (O_2) and an increase in the salinity of STUW. They suggested that the changes of the water mass are due to the surface warming and salinification at the formation site in the central North Atlantic under the North Atlantic Oscillation (NAO) and the Atlantic Multidecadal Oscillation (AMO) forcings. Decadal and longer-term trends in global STUW were also noted by other studies (e.g., Hasson et al., 2013; O'Connor et al., 2002; Polovina et al., 2008; Zhang & Qu, 2014).

STUW has relatively short residence time (<10 years), and its connection to the tropical and subpolar regions via interior pathways can impart the subtropical salinity influence to both the equatorial thermocline (Fine et al., 2001; Gu & Philander, 1997; McCreary & Lu, 1994; Zhang et al., 2003) and the North Atlantic Deep Water (Burkholder & Lozier, 2011; Qu et al., 2013). Because of these broad-scale impacts of STUW, there has been growing interest in the cause of its decadal trends. The STUW properties are determined by its last contact with the atmosphere in the formation region, and these properties result from the mixed layer processes that are forced by local atmospheric wind and buoyancy forcing, lateral mixing, or ocean eddy transport (Qiu & Huang, 1995; Williams, 1991). It has been known that the salinities in the subtropical North Atlantic have increased in the past 50 years (Boyer et al., 2005; Curry et al., 2003; Durack & Wijffels, 2010; Rosenheim et al., 2005). The trend is seen as supporting evidence of the "dry-gets-drier and wet-gets-wetter" (DDWW) paradigm (Held & Soden, 2006) over the ocean (Byrne & O'Gorman, 2015), indicating that the global water cycle amplifies as a consequence of the Clausius-Clapeyron increase in water vapor transport (Seager et al., 2010). In tandem, a new, independent mechanism has emerged, showing that the exacerbation of the subtropical dry zones since 1979 is the result of a poleward shift of midlatitude jet stream and storm tracks (Lu et al., 2007; Scheff & Frierson, 2012; Yin, 2005). The shift drives poleward expansion of the subtropical dry zones and the descending branch of the Hadley circulation (HC), leading to a widening of the tropical belt (Fu et al., 2006; Hudson et al., 2006; Seidel et al., 2008). Scheff and Frierson (2012) examined the two mechanisms in the Coupled Model Intercomparison Project phase 3 (CMIP3) models and suggested that in the HC expansion scenario, the poleward side of the subtropical dry zones is dried, while the equatorward side is not changed. In essence, the HC expansion mechanism affects poleward edges of the subtropical zones, whereas the DDWW mechanism emphasizes the thermodynamic amplification of the dry-wet contrast.

In this study, we report the findings that the recent decadal changes in the STUW properties of the North Atlantic resulted from poleward expansion of the SSS-max. We present the observations to show that the expansion of the SSS-max has shifted the ventilation of STUW poleward, causing the core of STUW to expand and its salinity to increase.

2. Method

The monthly objectively analyzed subsurface temperature and salinity by Ishii et al. (2006) is used. The objectively analyzed fields cover the global oceans with horizontal resolution of 1° × 1° and 24 levels in the upper 1,500 m for the period from 1945 up to 2012. The topmost level is set at 10 m below the surface. Hence, SSS in this study refers to a salinity near the surface. Detailed information on input data sources used in the compilation and associated quantification of sampling errors and statistical errors are provided in Ishii et al. (2006). This study focuses on the period from 1979 onward, which is the period that poleward expansion of HC is documented (Seidel et al., 2008). The study area is the North Atlantic subtropical gyre between 5°N and 50°N in latitude and between 80°W and 0 in longitude.

The SSS-max center is defined as the water mass enclosed by the surface 37 isohaline contour. The STUW formation area, subduction rate, and volume were constructed for the water mass that satisfies the ranges of salinity (36.7–37.2) and potential temperature (20.4–22.2°C), with equivalent densities from 25.6 to 26.3 kg m^{-3} (O'Connor et al., 2005). The mixed layer depth was computed from the monthly temperature and salinity fields, using the criterion that the base of the mixed layer is the depth at which density is 0.125 kg m^{-3} higher than the surface density (Monterey & Levitus, 1997).

3. Results

3.1. Poleward Expansion of the SSS-max

Two sets of metrics are used to depict the decadal changes of the SSS-max in the North Atlantic (Figure 1a): the mean salinity patterns for the two 10 year epochs, 1980–1989 and 2000–2009 (denoted by the respective

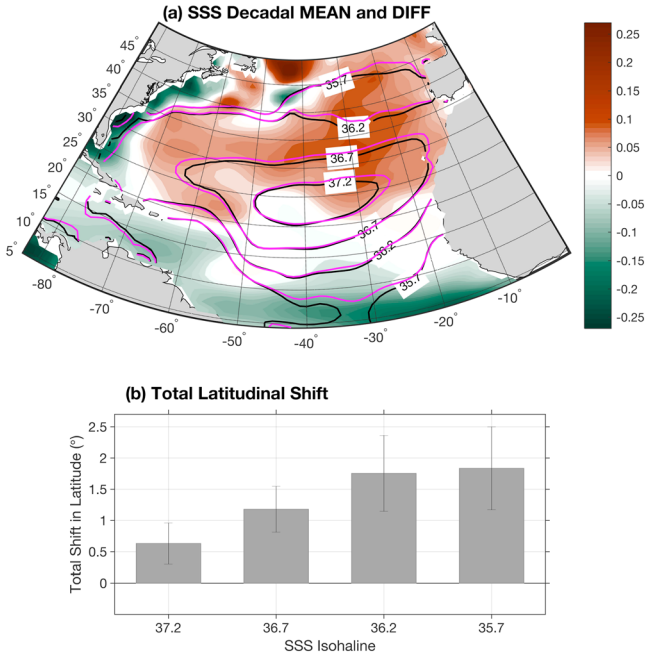

Figure 1. (a) Mean SSS in the subtropical North Atlantic in the 1980s (black contours) and the 2000s (magenta contours) with the SSS mean differences between the two decades in the background (colors). (b) The total shift in the positions of the selected isohalines located north of 25°N, with error bars denoting the 95% confidence interval estimates.

black and magenta contours), and the mean salinity differences between the two decades (denoted by the colored background). Using the SSS-max center location at 25°N as a reference, the northern outer boundary (i.e., the isohalines north of 25°N) has expanded northward while the southern outer boundary has changed only slightly. As a result, there is a latitudinal asymmetry in SSS anomalies across the SSS-max center, with significant salinification of the sea surface (positive anomalies) on the northern edge and slight freshening of the sea surface (negative anomalies) on the southern edge of our domain. It appears that the expansion shifted the SSS-max water northeastward and caused a freshening on the southwestern side of the SSS-max center. The surface freshening was most significant at the near-equatorial latitudes, where the slight northward displacement of 35.7 isohalines seems to be associated with the change of the tropical rainfall pattern.

The degree of latitudinal shift was quantified for the isohalines, from 37.2 down to 35.7 with 0.5 interval, on the northern edge of the SSS-max center (Figure 1b). The grid points near the western boundary points were excluded in the computation. Linear trends were derived, and the total latitudinal shift was obtained by multiplying the total 34 years (1979–2012). The northward shift is smallest in the center of the SSS-max (the 37.2 isohaline), a total of 0.63 ± 0.33° latitude over the 34 years, and greatest for the 35.7 isohaline, a total of 1.8 ± 0.67° latitude. The edge of the STUW outcrop 36.7 isohaline has shifted northward by 1.2 ± 0.36° latitude, equivalent to 0.35 ± 0.11° latitude per decade. The linear trend is derived from linear regression, and the error bar represents the difference between the upper and lower confidence limits at the 95% confidence interval for the fitted value.

Data coverage is inhomogeneous in the Ishii product, as the number of the SSS observations is augmented significantly since Argo became available after 2002. To verify the potential impacts of data coverage on our finding, we have conducted analysis using the 5 year composite mean of the World Ocean Database (WOD) (Boyer et al., 2005) and the HydroBase (Curry & Nobre, 2013; http://www.whoi.edu/hydrobase/php/index.php#). A shift of the SSS-max center is shown in all products, albeit the magnitude varies. We have further used the SSS observations from the Ship of Opportunities maintained by the Laboratoire d Etudes en Geophysique et Oceanographie Spatiale (LEGOS), Toulouse, France (Reverdin et al., 2007; http://www.legos.obs-mip.fr/observations/sss), and the comparison is shown in supporting information Figure S1.

3.2. Poleward Shift in the Ventilation of STUW

The northward shift of the outcrop 36.7–37.2 isohalines (Figure 1b) would lead to changes in the subduction rate of the STUW. The subduction rate is computed here as positive downward to denote the downward transport of the mass flux from the mixed layer to the permanent pycnocline. Following Qiu and Huang (1995), the annual subduction rate, S_{ann}, can be approximated using the mixed-layer properties:

$$S_{ann} = -\frac{1}{T}\int_{T_1}^{T_2}\left(w_{EK} - \frac{\beta}{f}\int_{-h_m}^{0} v_g dz\right) dt - \frac{1}{T}\left(h_m(T_2) - h_m(T_1)\right) \quad (1)$$

where T is 1 year, and T_1 and T_2 are the end of the first and second winters, respectively, and commonly set to March. w_{EK} is the Ekman pumping velocity and was computed from satellite-based wind stress product from the Objectively Analyzed air-sea Fluxes (OAFlux) project (Yu & Jin, 2014). The β term denotes the vertical velocity reduction due to the meridional velocity v_g in the surface layer, and v_g was computed from the thermal wind equations using the Ishii temperature and salinity analysis. We assumed a level of no motion at 2,000 m depth. $h_m(T_1)$ and $h_m(T_2)$ denote the mixed-layer depth in the first and second winters at its respective release and destination locations along a Lagrangian trajectory. The particle is traced along the isopycnals for 1 year from the time it is subducted. If the particle reenters the mixed layer at any time of the year, it is discarded. If it

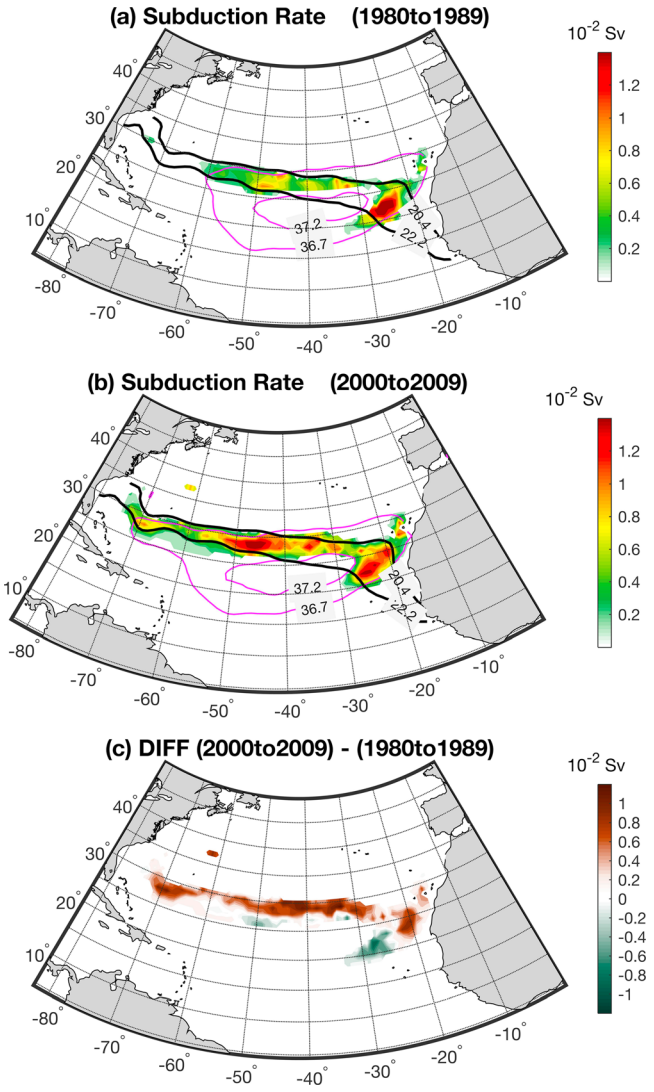

Figure 2. Annual mean subduction rate (colors) in (a) the 1980s, (b) the 2000s, and (c) the differences between the two decades (i.e., 2000s minus 1980s). In Figures 2a and 2b, black contours denote the 20.4 and 22.2°C outcrop isotherms in March and magenta contours denote the 36.7 and 37.2 outcrop isohalines in March for the respective decade.

remains submerged below the mixed layer after 1 year, the subduction rate along with the position and time is then recorded.

For computations based on monthly data sets, subduction at most STUW formation sites does not always commence in March (Liu & Huang, 2011), although March is the most productive month over the calendar year. To improve the approximation of the subduction rate, we adopted the original equation in Qiu and Huang (1995), which was established from the instant detrainment rate, D. We traced the trajectory of the water parcel for 1 year from the time that it is released at the base of the mixed layer. If the parcel reenters the mixed layer at any time of the 1 year tracking period, the detrainment rate of the parcel is discarded. Hence, only the effective detrainment contributes to subduction. The total subduction rate estimated from this approach can be expressed in Eulerian coordination:

$$S_{\mathrm{ann}} = -\frac{1}{T}\int_{T_1}^{T_2} D\,\mathrm{d}t = -\frac{1}{T}\int_{T_1}^{T_2} w_{\mathrm{tr}}\,\mathrm{d}t - \frac{1}{T}\int_{T_1}^{T_2}\left(\mathbf{u}_{tr}\cdot\nabla h_m + \frac{\partial h_m}{\partial t}\right)\mathrm{d}t \quad (2)$$

where w_{tr} and u_{tr} are the vertical and horizontal velocities along the trajectories. T is still 1 year, while T_1 and T_2 are the times when effective detrainment starts and ends. The first integral term in equation (2) represents the effect of the vertical velocity across the base of the mixed layer, and the second integral term represents lateral induction due to the slope of the mixed layer base. Integrating S_{ann} over the ventilation zone at the surface yields an annual subduction rate with units in sverdrup (Sv; 1 Sv = 10^6 m^3 s^{-1}).

The spatial distribution of S_{ann} averaged over the decades of the 1980s and 2000s as well as the difference in S_{ann} between the two decades were constructed (Figures 2a–2c). In the former two patterns, the bounding isohaline and isotherm outcrops in March of the respective decade are superimposed. The annual mean subduction region falls well within the isohaline and isotherm outcrops in March, supporting the notion that the ventilation occurs mostly during March–April when the mixed layer shoals and restratifies (Stommel, 1979). The narrow subduction zone stretched across the basin at 25–30°N latitudes, tilting southeastward at the eastern end (east of 30°W). Compared to the 1980s, S_{ann} in the 2000s was stronger, westward expanded, and northward shifted. The band of positive (stronger) S_{ann} anomalies at ~30°N predominates over the band of negative (weaker) S_{ann} anomalies that is bordered to the south (Figure 2c). The westward expansion of the subduction site into the Sargasso Sea is particularly noteworthy, as this is a place where STUW was rarely formed in the 1980s. This westward intrusion of the subduction site could have been the direct result of the expansion of the SSS-max, both northward and westward. For instance, the westernmost edge of the 36.7 isohaline has extended by as much as 10° longitude westward, from near 60°W in the 1980s to 70°W and beyond in the 2000s (Figures 2a and 2b). The finding of the westward expansion of the SSS-max was unexpected. This expansion occurred in a narrow latitudinal band between 25 and 35°N (Figure 1a), collocating with the formation site of the North Atlantic subtropical mode water (Hanawa & Talley, 2001). We suspect that ocean internal dynamics might play a role in the westward amplification of the HC shift.

Year-to-year variability of S_{ann} shows that the production of STUW has trended up during the three decades in analysis (Figure 3a). The trend was steadily upward in the 1980s and 1990s but flattened out in the 2000s. The overall rate of increase is 0.31 (or 35%) ± 0.20 Sv per decade, amounting to a total of 1.02 Sv increase in S_{ann} in 34 years. Given the uncertainties in Ishii data set for the pre-Argo period, the statistical significance of the trend might be weak. Partition of the contributions from the two integral terms in equation (2) suggests

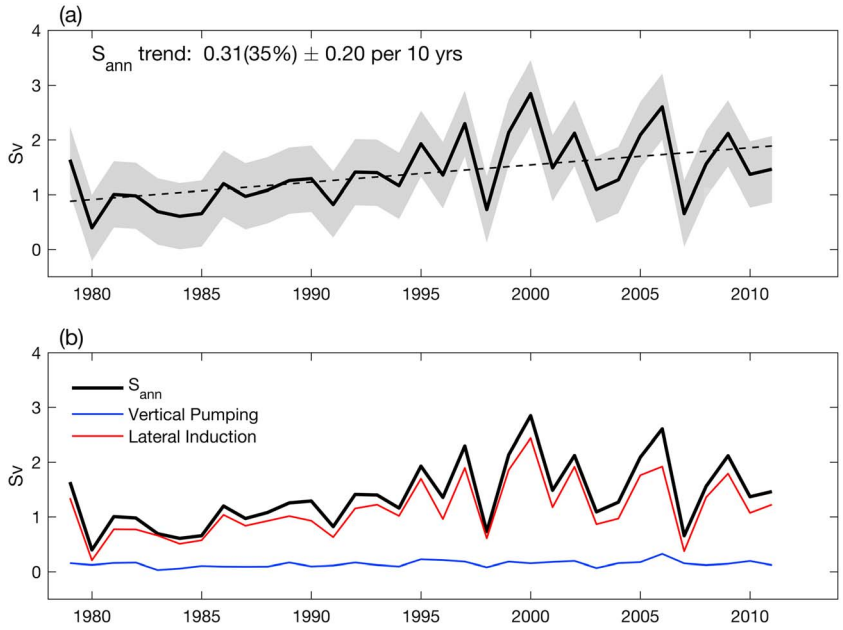

Figure 3. (a) Time series of annual mean subduction rate. The shaded error bands denote one standard deviation of annual variability. (b) Time series of annual mean subduction rate (black) and the respective contributions from vertical pumping (blue) and lateral induction (red).

that the lateral induction of the sloping mixed layer is the dominant contributor to the interannual-to-decadal variability of S_{ann} and the contribution from the vertical pumping velocity across the base of the mixed layer is small (Figure 3b). Qiu and Huang (1995) pointed out that the annual excursion of the mixed layer depth greatly exceeds the vertical Ekman pumping. As a result, the subduction rates are governed primarily by the rapid shoaling of the mixed-layer depth in response to surface buoyancy gain (Kolodziejczyk et al., 2015; Liu & Huang, 2011; Trossman et al., 2009). Qu et al. (2016) provided additional evidence for the sensitivity of STUW to the mixed layer change: STUW is produced at the intersection of the mixed layer front (or the mixed layer sharp transition zone) and the outcrop isohalines. As the winter-spring mixed layers show a deepening by 10–40 m in the past 50 years (1945–2004) (Carton et al., 2008), it would not be a surprise to learn that the global subduction rates have simultaneously increased by 8% by the lateral induction mechanism (Liu & Huang, 2011). Our estimated trend in the STUW subduction rate during 1979–2012 is in keeping with the trends found in the global subduction rates.

It is worth pointing out that although the STUW subduction is expected to play a vital role in moving the surface water into the ocean interior, the role of submesoscale processes should not be ignored. The observations obtained from the Salinity Processes in the Upper Ocean Regional Study—1 (SPURS-1) field program showed that the STUW subduction is highly variable and inhomogeneous, featuring seasonal intensification of interleaving in late spring (Shcherbina et al., 2015). The parameterization of S_{ann} (equations (1) and (2)) and the gridded products provide only the bulk information associated with the STUW subduction.

3.3. Expansion of the STUW

STUW is advected southward and southwestward along the 25.6–26.3 kg m^{-3} isopycnals as part of the subtropical gyre. The mean depth at which the STUW is located was determined as the depth-weighted mean for the depths associated with the 25.6–26.3 kg m^{-3} isopycnals. We computed the mean depth at each grid and for each month, from which we constructed the mean-depth patterns in the 1980s and 2000s and the differences between the two decadal patterns (Figures 4a and 4b). The spatial distribution of the STUW depth shows that the capped high-salinity water mass descends deeper as it moves south and southward away from where it outcrops and sinks down to the depth of ~180 m near the Caribbean islands at 20°N. Compared to the 1980s, the water mass in the 2000s shows expansion, both northward and westward (see the stippled areas in Figure 4). This can be from the northward displacement of the 60 m isoline from the

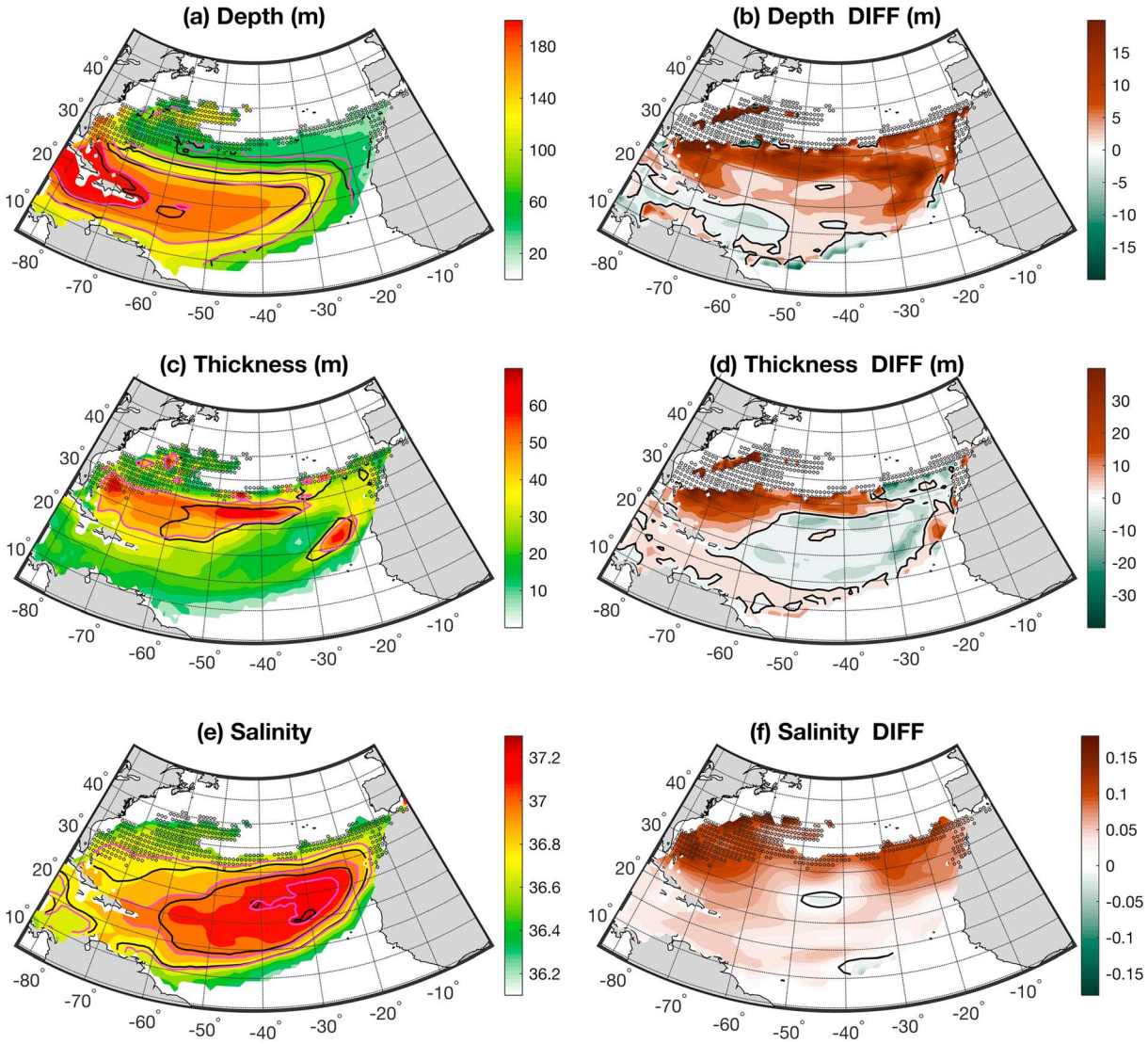

Figure 4. (a) Mean depth of STUW in the 1980s (black contours) and the 2000s (colors and red contours). The contour lines are the isolines from 60 m to 180 m at 40 m intervals. (b) The 2000s minus 1980s anomalies in the depth of STUW. (c) STUW layer thickness in the 1980s (black contours) and the 2000s (colors and red contours). The contoured lines are the 40 m isolines. (d) The 2000s minus 1980s anomalies in the layer thickness. (e) Mean STUW salinity in the 1980s (black contours) and the 2000s (colors and red contours). The contoured lines are the 36.7, 36.9, and 37.1 isohalines. (f) The 2000s minus 1980s anomalies in the STUW salinity. In Figures 4b, 4d, and 4f, zero contours are highlighted. In Figures 4a–4f, the stippled areas denote the areas existing only in the 2000s as a result of the STUW expansion.

1980s to the 2000s. Substantial STUW water was formed in the western subtropical basin in the 2000s, which was not seen in the 1980s. Some water mass subducted to the west of 60°W turned northward, showing a core depth of ~120 m near 40°N, which is about 10° northward of the formation site.

For the two decadal patterns in comparison (Figure 4b), the vertical distribution of the STUW core has deepened by 10–15 m in a distinct zonal band near the ventilation zone. As the STUW sank southward and southwestward away from the ventilation zone, the deepening of the vertical location was much reduced. Near the Caribbean Sea the deep core has even slightly shallowed. The STUW core in the formation region has become not only deeper but also thicker (Figures 4c and 4d), which can be attributed to the increased S_{ann} anomalies at the ventilation latitudes (Figure 2) that caused more salty water to be fluxed into the pycnocline. In this study, the layer thickness was determined by the depth differences corresponding to the depths associated with the 25.6 and 26.3 kg m^{-3} isopycnals. The mean spatial pattern of the STUW thickness features two thick

bands, one in the central basin along the 30°N latitude and the other in the east aligned southwestward. The two bands of thick STUW layers are collocated with the sites of the maximum S_{ann} (Figure 2). Ventilation west of 60°W in the 2000s pushed the STUW formation westward along the 30°N latitude, expanding westward the pool of STUW with thickness of 40 m. In addition, the northward shift of the core subduction site (Figure 2c) has shifted the location of the two thick bands northward (Figure 4d), which caused a slight reduction in the layer thickness in the gyre interior. The deepening and thickening of STUW on its northern and western boundaries are the two most noted features of the effects of the poleward expansion of the SSS-max on the ventilation of STUW.

Projecting the salinity changes associated with the three-dimensional changes of STUW is challenging, as the water mass did not stay at the same vertical level but sank deeper and grew thicker. To take into account the effects of the changes of the vertical distribution on salinity, we attempted to construct the salinity change within a depth range that is fixed at each grid location. To do so, we first obtained the depths associated with the 25.6 and 26.3 kg m^{-3} isopycnals over the 34 years and used the shallowest and deepest depths over the entire period as the upper and lower boundaries of the STUW vertical fluctuations at the chosen grid location. The STUW salinity variability confined within this depth range was averaged. The spatial distribution of the salinity thus constructed displays a salinity maximum pool centered in the northeast of the subtropical gyre, with the salinity decreasing toward the southwest (Figure 4e). From the 1980s to the 2000s, the salinity pattern shows a northward and westward expansion on the northern edge of the high-salinity core and little or no significant changes on the southern edge. The expansion was the result of the shift in the ventilation zone and the occurrence of the STUW formation west of 60°W. The subsequent effects are the enlarged spatial extent of the vertical salinity core, with significant salinity increase, up to 0.15, in the northern and western outer boundaries and a slight reduction in the center (Figure 4f). The pattern of change supports the notion (Montes et al., 2016) that the STUW became saltier in the recent decade.

4. Summary and Conclusion

We report the findings that the sea surface salinity maximum (SSS-max) in the North Atlantic has poleward expanded in recent decades and that the expansion is a main driver of the decadal changes in subtropical underwater (STUW). Using the temperature and salinity analysis by Ishii et al. (2006), we show that the expansion caused the ventilation zone (marked by the location of the 36.7 isohaline) to be displaced northward by 1.2 ± 0.36° latitude for the 34 year (1979–2012) period and caused SSS to increase by up to 0.1 on the northern edge and decrease in the center and on the southern edge. In responding to the redistribution of the high saline surface water, the ventilation of STUW not only shifted northward but also expanded westward to the western subtropical basin that had little or no STUW production in the 1980s.

The annual subduction rate shows an upward trend of 0.31 (or 35%) ± 0.20 Sv per decade, amounting to a total of 1.02 Sv increase in 34 years. The trend was steadily upward in the 1980s and 1990s but flattened out in the 2000s. The increased subduction rate was due primarily to the lateral induction of the sloping mixed layer, perhaps in relation to the observed winter mixed-layer deepening that was previously reported. The enhanced ventilation rate, together with the northward shifted and westward enlarged ventilation zone, have affected the three-dimensional distribution of the vertical salinity maximum water. The high-saline core of the STUW expanded northward and westward, increasing the salinity by up to 0.15 on the northern and western edges of the core, and meanwhile, the layer of the STUW became deeper and thicker.

The present study was based primarily upon the salinity and temperature analysis by Ishii et al. (2006). Quantification of the changes in the STUW properties is subject to several uncertainty factors, including the temporal and spatial inhomogeneity of data sampling, the low horizontal and temperature resolutions that prevent eddy resolving, the choice of the criterion used in determining the mixed layer depth, and the approximation used in defining the subduction rate. Furthermore, the sensitivity of S_{ann} to the reference level of no motion at the depths of 1,000 m and 1,500 m was examined. The results show that the impacts of the reference level is negligible, because S_{ann} is determined primarily by the lateral induction. Our analysis offers the first-order depiction of the change of the STUW in the context of the poleward shift of the SSS-max.

Acknowledgments
The study was supported by the NOAA Ocean Observation and Monitoring Division (OOMD) under grant NA14OAR4320158. The Ishii subsurface salinity and temperature analyses was downloaded from https://rda.ucar.edu/datasets/ds285.3/. The OAFlux high-resolution vector wind analysis is available at http://oaflux.whoi.edu.

References

Bingham, F. M., Busecke, J., Gordon, A. L., Giulivi, C. F., & Li, Z. (2014). The North Atlantic subtropical surface salinity maximum as observed by Aquarius. *Journal of Geophysical Research: Oceans*, *119*, 7741–7755. https://doi.org/10.1002/2014JC009825

Blanke, B., Arhan, M., Lazar, A., Mignot, J., & Prévost, G. (2002). A Lagrangian numerical investigation of the origins and fates of the salinity maximum water in the Atlantic. *Journal of Geophysical Research*, *107*(C10), 3163. https://doi.org/10.1029/2002JC001318

Boyer, T. P., Levitus, S., Antonov, J. I., Locarnini, R. A., & Garcia, H. E. (2005). Linear trends in salinity for the world ocean, 1955–1998. *Geophysical Research Letters*, *32*, L01604. https://doi.org/10.1029/2004GL021791

Bryan, F., & Bachman, S. (2014). Isohaline salinity budget of the North Atlantic salinity maximum. *Journal of Physical Oceanography*, *45*, 724–736. https://doi.org/10.1175/JPO-D-14-0172.1

Burkholder, K. C., & Lozier, M. S. (2011). Subtropical to subpolar pathways in the North Atlantic: Deductions from Lagrangian trajectories. *Journal of Geophysical Research*, *116*, C07017. https://doi.org/10.1029/2010JC006697

Byrne, M. P., & O'Gorman, P. A. (2015). The response of precipitation minus evapotranspiration to climate warming: Why the "wet-get-wetter, dry-get-drier" scaling does not hold over land. *Journal of Climate*, *28*(20), 8078–8092. https://doi.org/10.1175/JCLI-D-15-0369.1

Carton, J. A., Grodsky, S. A., & Liu, H. (2008). Variability of the oceanic mixed layer, 1960–2004. *Journal of Climate*, *21*(5), 1029–1047. https://doi.org/10.1175/2007JCLI1798.1

Curry, R., Dickson, B., & Yashayaev, I. (2003). A change in the freshwater balance of the Atlantic Ocean over the past four decades. *Nature*, *426*(6968), 826–829. https://doi.org/10.1038/nature02206

Curry, R., & Nobre, C. (2013). Hydrobase3, Technical Report, 38 Pp., Woods Hole Oceanogr. Inst. [Available at http://www.whoi.edu/hydrobase/docs/TechReport_03Sep2013.pdf.]

Durack, P. J., & Wijffels, S. E. (2010). Fifty-year trends in global ocean salinities and their relationship to broad-scale warming. *Journal of Climate*, *23*(16), 4342–4362. https://doi.org/10.1175/2010JCLI3377.1

Fine, R. A., Maillet, K. A., Sullivan, K. F., & Willey, D. (2001). Circulation and ventilation flux of the Pacific Ocean. *Journal of Geophysical Research*, *106*(C10), 22,159–22,178. https://doi.org/10.1029/1999JC000184

Fu, Q., Johanson, C. M., Wallace, J. M., & Reichler, T. (2006). Enhanced mid-latitude tropospheric warming in satellite measurements. *Science*, *312*(5777), 1179. https://doi.org/10.1126/science.1125566

Gordon, A. L., Giulivi, C., Busecke, J., & Bingham, F. M. (2015). Differences among subtropical surface salinity patterns. *Oceanography*, *28*(1), 32–39. https://doi.org/10.5670/oceanog.2015.02

Gu, D., & Philander, S. G. H. (1997). Interdecadal climate fluctuations that depend on exchange between the tropics and extratropics. *Science*, *275*(5301), 805–807. https://doi.org/10.1126/science.275.5301.805

Hanawa, K., & Talley, L. D. (2001). Mode waters. In G. Siedler, J. Church, & J. Gould (Eds.), *Ocean circulation and climate: Observing and modelling the global ocean*, *international geophysics series* (Vol. 77, pp. 373–386). London: Academic Press. https://doi.org/10.1016/S0074-6142(01)80129-7

Hasson, A., Delcroix, T., & Boutin, J. (2013). Formation and variability of the South Pacific Sea surface salinity maximum in recent decades. *Journal of Geophysical Research: Oceans*, *118*, 5109–5116. https://doi.org/10.1002/jgrc.20367

Held, I., & Soden, B. (2006). Robust responses of the hydrological cycle to global warming. *Journal of Climate*, *19*(21), 5686–5699. https://doi.org/10.1175/JCLI3990.1

Hernández-Guerra, A., & Joyce, T. M. (2000). Water masses and circulation in the surface layers of the Caribbean at 66°W. *Geophysical Research Letters*, *27*(21), 3497–3500. https://doi.org/10.1029/1999GL011230

Hudson, R. D., Andrade, M. F., Follette, M. B., & Frolov, A. D. (2006). The total ozone field separated into meteorological regimes, part II: Northern Hemisphere mid-latitude total ozone trends. *Atmospheric Chemistry and Physics*, *6*(12), 5183–5191. https://doi.org/10.5194/acp-6-5183-2006

Ishii, M., Kimoto, M., Sakamoto, K., & Iwasaki, S.-I. (2006). Steric sea level changes estimated from historical ocean subsurface temperature and salinity analyses. *Journal of Oceanography*, *62*(2), 155–170. https://doi.org/10.1007/s10872-006-0041-y

Kolodziejczyk, N., Reverdin, G., & Lazar, A. (2015). Interannual variability of the mixed layer winter convection and spice injection in the eastern subtropical North Atlantic. *Journal of Physical Oceanography*, *45*(2), 504–525. https://doi.org/10.1175/JPO-D-14-0042.1

Liu, L., & Huang, R. X. (2011). The global subduction/obduction rates, their interannual and decadal variability. *Journal of Climate*, *25*, 1096–1115.

Lu, J., Vecchi, G. A., & Reichler, T. J. (2007). Expansion of the Hadley cell under global warming. *Geophysical Research Letters*, *34*, L06805. https://doi.org/10.1029/2006GL028443

Luyten, J. R., Pedlosky, J., & Stommel, H. M. (1983). The ventilated thermocline. *Journal of Physical Oceanography*, *13*(2), 292–309. https://doi.org/10.1175/1520-0485(1983)013%3C0292:TVT%3E2.0.CO;2

McCreary, J. P., & Lu, P. (1994). On the interaction between the subtropical and the equatorial oceans: The subtropical cell. *Journal of Physical Oceanography*, *24*, 466–497.

Monterey, G., & Levitus, S. (1997). Seasonal variability of mixed layer depth for the World Ocean. NOAA Atlas NESDIS 14, 100 pp.

Montes, E., Muller-Karger, F. E., Cianca, A., Lomas, M. W., Lorenzoni, L., & Habtes, S. (2016). Decadal variability in the oxygen inventory of North Atlantic subtropical underwater captured by sustained, long-term oceanographic time series observations. *Global Biogeochemical Cycles*, *30*, 460–478. https://doi.org/10.1002/2015GB005183

O'Connor, B. M., Fine, R. A., Maillet, K. A., & Olson, D. B. (2002). Formation rates of subtropical underwater in the Pacific Ocean. *Deep Sea Research Part I*, *49*(9), 1571–1590.

O'Connor, B. M., Fine, R. A., & Olson, D. B. (2005). A global comparison of subtropical underwater formation rate. *Deep Sea Research*, *52*(9), 1569–1590. https://doi.org/10.1016/j.dsr.2005.01.011

Polovina, J. J., Howell, E. A., & Abecassis, M. (2008). Ocean's least productive waters are expanding. *Geophysical Research Letters*, *35*, L03618. https://doi.org/10.1029/2007GL031745

Qiu, B., & Huang, R. X. (1995). Ventilation of the North Atlantic and North Pacific: Subduction versus obduction. *Journal of Physical Oceanography*, *25*, 2374–2390.

Qu, T., Gao, S., & Fukumori, I. (2013). Formation of salinity maximum water and its contribution to the overturning circulation in the North Atlantic as revealed by a global general circulation model. *Journal of Geophysical Research: Oceans*, *118*, 1982–1994. https://doi.org/10.1002/jgrc.20152

Qu, T., Zhang, L., & Schneider, N. (2016). North Atlantic subtropical underwater and its year-to-year variability in annual subduction rate during the Argo period. *Journal of Physical Oceanography*, *46*(6), 1901–1916. https://doi.org/10.1175/JPO-D-15-0246.1

Reverdin, G., Kestenare, E., Frankignoul, C., & Delcroix, T. (2007). Surface salinity in the Atlantic Ocean (30°S–50°N). *Progress in Oceanography*, *73*(3-4), 311–340. https://doi.org/10.1016/j.pocean.2006.11.004

Rosenheim, B. E., Swart, P. K., Thorrold, S. R., Eisenhauer, A., & Willenz, P. (2005). Salinity change in the subtropical Atlantic: Secular increase and teleconnections to the North Atlantic Oscillation. *Geophysical Research Letters*, *32*, L02603. https://doi.org/10.1029/2004GL021499

Scheff, J., & Frierson, D. (2012). Twenty-first-century multimodel subtropical precipitation declines are mostly midlatitude shifts. *Journal of Climate*, *25*(12), 4330–4347. https://doi.org/10.1175/JCLI-D-11-00393.1

Schmitz, W. J., & Richardson, P. L. (1991). On the sources of the Florida Current. *Deep Sea Research*, *38*(Suppl), 379–409.

Seager, R., Naik, N., & Vecchi, G. A. (2010). Thermodynamic and dynamic mechanisms for large-scale changes in the hydrological cycle in response to global warming. *Journal of Climate*, *23*(17), 4651–4668. https://doi.org/10.1175/2010JCLI3655.1

Seidel, D. J., Fu, Q., Randel, W. J., & Reichler, T. J. (2008). Widening of the tropical belt in a changing climate. *Nature Geoscience*, *1*, 21–24.

Shcherbina, A. Y., D'Asaro, E. A., Riser, S. C., & Kessler, W. S. (2015). Variability and interleaving of upper-ocean water masses surrounding the North Atlantic salinity maximum. *Oceanography*, *28*(1), 106–113. https://doi.org/10.5670/oceanog.2015.12

Stommel, H. M. (1979). Determination of water mass properties of water pumped down from the Ekman layer to the geostrophic flow below. *Proceedings of the National Academy of Sciences of the United States of America*, *76*(7), 3051–3055. https://doi.org/10.1073/pnas.76.7.3051

Trossman, D. S., Thompson, L., Kelly, K. A., & Kwon, Y.-O. (2009). Estimates of North Atlantic ventilation of mode water formation for winters 2002–06. *Journal of Physical Oceanography*, *39*(10), 2600–2617. https://doi.org/10.1175/2009JPO3930.1

Williams, R. G. (1991). The role of the mixed layer in setting the potential vorticity of the main thermocline. *Journal of Physical Oceanography*, *21*, 1802–1814.

Worthington, L. V. (1976). *On the North Atlantic circulation* (p. 110). Baltimore, MD: Johns Hopkins University Press.

Yin, J. (2005). A consistent poleward shift of the storm tracks in simulations of 21st century climate. *Geophysical Research Letters*, *32*, L18701. https://doi.org/10.1029/2005GL023684

Yu, L., & Jin, X. (2014). Insights on the OAFlux ocean surface vector wind analysis merged from scatterometers and passive microwave radiometers (1987 onward). *Journal of Geophysical Research: Oceans*, *119*, 5244–5269. https://doi.org/10.1002/2013JC009648

Zhang, D., McPhaden, M. J., & Johns, W. E. (2003). Observational evidence for flow between the subtropical and tropical Atlantic: The Atlantic tropical cells. *Journal of Physical Oceanography*, *33*(8), 1783–1797. https://doi.org/10.1175/2408.1

Zhang, L., & Qu, T. (2014). Low-frequency variability of South Pacific tropical water from Argo. *Geophysical Research Letters*, *41*, 2441–2446. https://doi.org/10.1002/2014GL059490